

NASA Technical Memorandum 100896  
AIAA-88-3180

# An Empirical Model of the Effects of Curvature and Convergence on Dilution Jet Mixing

James D. Holdeman  
*Lewis Research Center  
Cleveland, Ohio*

Ram Srinivasan and Craig D. White  
*Allied-Signal Aerospace Company  
Garrett Engine Division  
Phoenix, Arizona*

Prepared for the  
24th Joint Propulsion Conference  
cosponsored by the AIAA, ASME, SAE, and ASEE  
Boston, Massachusetts, July 11-13, 1988

**NASA**

AN EMPIRICAL MODEL OF THE EFFECTS OF CURVATURE AND CONVERGENCE  
ON DILUTION JET MIXING

James D. Holdeman\*  
National Aeronautics and Space Administration  
Lewis Research Center  
Cleveland, Ohio

and

Ram Srinivasan† and Craig D. White‡  
Allied-Signal Aerospace Company  
Garrett Engine Division  
Phoenix, Arizona

Abstract

An existing empirical model for the temperature field downstream of single and multiple rows of jets injected into a confined crossflow has been extended to model the effects of curvature and convergence on the mixing. This extension is based on the results of a numerical study of these effects using a three-dimensional turbulent flow computer code. Temperature distributions calculated with the empirical model are presented to show the effects of flow area convergence, radius of curvature, and inner and outer wall injection for single and opposed rows of jets.

Nomenclature

$AR$  orifice aspect ratio (width/length)  
 $A_j/A_m$  jet-to-mainstream area ratio for each row,  
 $(\pi/4)/[(S/H_0)(H_0/D)^2]$   
 $C$   $(S/H_0)\sqrt{J}$ ; Eq. (5)  
 $C_d$  orifice discharge coefficient  
 $D$  orifice diameter

$DR$  density ratio,  $T_m/T_j$   
 $D_j$   $D\sqrt{C_d}$   
 $dH/dx$  duct convergence rate  
 $H_{eq}$  effective duct height;  $H_0$  except for opposed rows of jets with centerlines in-line; see appendix  
 $H_0$  duct height at injection plane  
 $J$  momentum-flux ratio,  $(DR)R^2$   
 $n$  number of holes around can; see Eq. (6)  
 $R$  velocity ratio,  $V_j/U_m$   
 $R_{ci}$  inner radius of curvature in  $x-r$  plane  
 $R_t$  inner radius of curvature at inlet in  $r-z$  plane  
 $r$  radial coordinate  
 $S$  spacing between adjacent orifices  
 $S_x$  spacing between orifice rows  
 $T$  temperature  
 $T_j$  jet temperature  
 $T_m$  mainstream temperature  
 $U_m$  inlet mainstream velocity  
 $V_j$  jet velocity  
 $W_{1/2}^+$  jet half-width below centerline (for top injection); see Fig. 4  
 $W_{1/2}^-$  jet half-width above centerline (for top injection); see Fig. 4

\*Senior Research Engineer, Member AIAA

†Supervisor, Combustion Engineering Sciences

‡Senior Development Engineer, Combustion Advanced Technology

$w_j/w_T$  jet-to-total mass flow ratio,

$$\frac{\sqrt{(DR)J} C_d(A_j/A_m)}{1 + \left[ \sqrt{(DR)J} C_d(A_j/A_m) \right]}$$

$x$  axial coordinate; 0 at orifice centerline  
 $y$  cross-stream (radial) coordinate; 0 at injection wall,  $y_c$  at location of maximum  $\theta$  in vertical profile; see Fig. 4  
 $z$  circumferential coordinate; 0 at jet centerplane  
 $\phi$  angle around inlet from beginning of turn (in  $x-r$  plane)  
 $\theta$   $(T_m - T)/(T_m - T_j)$ ; Eq. (1)  
 $\theta_c$  maximum temperature difference ratio in vertical profile; see Fig. 4  
 $\theta_{EB}$  equilibrium  $\theta$ ,  $w_j/w_T$   
 $\theta_{\min}^+$  minimum temperature difference ratio below centerline (for top injection); see Fig. 4  
 $\theta_{\min}^-$  minimum temperature difference ratio above centerline (for top injection); see Fig. 4

### Introduction

Several previous investigations on the mixing of jets injected into a ducted crossflow have been motivated by the need to design or tailor the temperature pattern at the combustor exit in gas turbine engines. Results from experimental and modeling studies of the mixing of single and multiple jets with an isothermal flow in a straight duct have been reported in Refs. 1 to 7. Flow and geometric variations typical of many gas turbine combustors, namely variable temperature mainstream, flow area convergence, and double or opposed rows of jets, either in-line or staggered have been reported in Refs. 8 to 13.

From the data in Ref. 14, an empirical model<sup>5,15</sup> was developed to predict the temperature field downstream of a row of jets injected into a confined crossflow. A micro-computer program based on this empirical model was used in Ref. 7 to investigate the effects of separately varying the independent flow and geometric variables and to identify the key variables and the relationships among them which characterized the mixing.

This empirical model was extended on the basis of experimental results to model the effects of a variable temperature mainstream, flow area convergence, noncircular orifices, and double rows of jets, both axially staged and opposed.<sup>11,13,16-19</sup> This model has demonstrated a very good predictive capability within the parameter range of the generating experiments.<sup>5,12</sup>

In addition to the evolution and extension of empirical modeling schemes, rapid advances have been made recently

in the capability of computational fluid dynamics models and their application to complex flows such as jet(s)-in-cross-flow.<sup>20-25</sup> These codes offer several advantages over purely empirical models, including the capability to predict all flowfield quantities (rather than only those for which empirical models exist), and the ability to consider flows outside the range of experiments, or flows where empirical assumptions are invalid.

An example of the capability and promise of this type of code is given in Ref. 12, where temperature field distributions calculated by using a three-dimensional, elliptic, viscous-flow code with a standard  $k-\epsilon$  turbulence model<sup>22</sup> are compared with measurements from selected cases in Ref. 15 and with distributions calculated by using the empirical model reported therein. The three-dimensional code calculations shown in Ref. 12 correctly approximated the trends from variation of the independent flow and geometric variables, but they consistently exhibited too little mixing. Although improvements in numerics, accuracy, and turbulence models should provide more quantitative predictions, there would appear to be a continuing need for the empirical model as a near-term design tool, provided that the conditions of interest are within the range of the experience on which the model is based.

One application for which existing data and empirical models are inadequate to characterize the mixing is the flowfield in the annular transition duct that connects the exit of the combustor to the inlet of the first-stage turbine in gas turbine engines using reverse-flow combustor configurations. A cross-section schematic of this type of engine with the transition duct highlighted is shown in Fig. 1. With the current trend toward shorter combustors, the transition duct not only must turn the flow direction 180° but also must efficiently mix the dilution air with the hot mainstream gases. A detailed understanding of the flowfield in the transition duct is essential to control the temperature profile entering the turbine.

Limited experimental studies of this flowfield have been reported in Refs. 26 and 27. Reference 28 summarizes results from computations given in Ref. 30, in which a three-dimensional, TEACH-type, turbulent, viscous-flow computer code was used to investigate the effects of transition duct curvature and convergence on the mixing of single and opposed rows of dilution jets.

In Ref. 30, the empirical model in Ref. 13 was revised to model the trends evident in the numerical calculations in Ref. 29. The current extension of this model retains all the capabilities of the earlier versions with the added capability to investigate the effects of curvature. Note that this model is an extension of an existing empirical model, thus retaining its demonstrated capabilities and limitations.<sup>18</sup> Also, the empirical model calculations (for dilution jet mixing in straight ducts) shown in Ref. 12 were in generally better quantitative

agreement with the data than three-dimensional numerical model calculations; therefore, the empirical model was extended to model only the trends, and not the quantitative results, from the numerical calculations.

### Description of the Flowfield

The basic geometry for the transition ducts used in the calculations performed in this study is shown in Fig. 2. The radius of curvature of the inner duct wall in the  $r$ - $z$  plane is given nondimensionally by its ratio to the inlet duct height  $R_i/H_0$ . The curved sections in the  $x$ - $r$  plane were generated by using circular arcs, and the curvature parameter was specified as the inner radius of curvature of the duct normalized by the inlet duct height  $R_{ci}/H_0$ . Possible transition ducts are defined by values of  $R_{ci}$  and  $R_i$  between zero and infinity. The limiting geometries defined by the possible values of the curvature parameters are as follows: a rectangular channel is defined if  $R_i$  and  $R_{ci}$  are infinite, a can results if  $R_{ci}$  is infinite and  $R_i=0$ , and an annular duct results if  $R_{ci}$  is infinite and  $0 < R_i < \infty$ .

The duct convergence was identified by the ratio of the exit cross-sectional area to that at the jet injection location. The primary independent flow and geometric variables, specified at the location where the dilution jets were injected into the mainstream flow, were the jet-to-mainstream momentum-flux ratio  $J$  and the orifice-spacing-to-duct-height ratio  $S/H_0$ . The orifice configurations for which calculations are presented in this paper are shown in Fig. 3. The range of variation of these independent flow and geometric variables is given in Table 1.

The calculated temperature levels are presented as centerplane and cross-stream contours of the nondimensional parameter

$$\theta = (T_m - T)/(T_m - T_j) \quad (1)$$

where  $T$  is the local mean temperature,  $T_m$  is the mainstream temperature, and  $T_j$  is the jet temperature. In the following paragraphs, cases are compared which differ from each other by a single parameter, so the effect of that parameter can be examined. The flow and geometry conditions for the cases discussed are given in Table 2. The case numbers shown correspond to those in Refs. 29 and 30.

### The Empirical Flowfield Model

The empirical model for the temperature field downstream of jets mixing with a confined crossflow is based on the observation that all vertical temperature profiles can be expressed in the following self-similar form:

$$\frac{\theta - \theta_{\min}^{\pm}}{\theta_c - \theta_{\min}^{\pm}} = \exp \left[ \frac{\ln 2(y - y_c)^2}{(W_{1/2}^{\pm})^2} \right] \quad (2)$$

where  $\theta$  is the local temperature difference ratio defined by Eq. (1), and  $\theta_c$ ,  $\theta_{\min}^+$ ,  $\theta_{\min}^-$ ,  $W_{1/2}^+$ ,  $W_{1/2}^-$ , and  $y_c$  are scaling parameters as shown in Fig. 4. Correlations have been developed for each of these in terms of the independent variables  $J$ ,  $S/D$ ,  $H_0/D$ ,  $z/S$ ,  $x/H_0$ ,  $S_x/H_0$ ,  $R_{ci}/H_0$ ,  $R_i/H_0$ , the mainstream temperature, and flow area convergence. The correlations used in the present version of the empirical model are given in Ref. 30. The complete set of correlation equations is given in the appendix. The most recent revisions to this model are given in the section Effects Due to Curvature in the appendix.

For all calculations, the flow and geometric variables that must be specified are the discharge coefficient, density ratio, momentum-flux ratio, orifice-spacing-to-duct-height ratio, duct-height-to-orifice-diameter ratio, the axial offset between rows, flow area convergence, orifice aspect ratio, radii of curvature, and mainstream temperature profile. Although calculations can be performed for most flow and geometric conditions of interest, they will be most reliable for conditions within the range of the experiments and calculations shown in Table 1. The density ratio, momentum-flux ratio, orifice spacing, orifice size, radii of curvature, and flow area convergence are the primary independent variables. Quantities derived from these, the orifice-to-mainstream area ratio, the jet-to-total mass flow split, and the parameter coupling the spacing and momentum-flux ratio, are also given in the table.

Table 1 Ranges of flow and geometric variables on which model is based

Independent variables	
Density ratio, $DR$ .....	0.5 to 2.2
Momentum-flux ratio, $J$ .....	5 to 105
Orifice spacing, $S/H_0$ .....	0.125 to 1
Orifice row offset, $S_m/H_0$ .....	0.25 to 0.5
Orifice aspect ratio .....	0.36 to 2.8
Orifice diameter, $D/H_0$ .....	0.0625 to 0.25
Area ratio (exit/inlet) .....	1 to $1/3$
Radius of curvature in $x$ - $r$ plane, $R_{ci}/H_0$ .....	0.25 to $\infty$
Radius of curvature in $x$ - $r$ plane, $R_i/H_0$ .....	0 to $\infty$
Variable mainstream, $\theta$ .....	0 to 0.5
Derived variables	
$A_j/A_m$ .....	0.025 to 0.1
$w_j/w_T$ .....	0.075 to 0.36
$C = (S/H_0) \sqrt{J}$ .....	0.5 to 10

Table 2 Flow and geometry conditions

Figure	Case <sup>a</sup>	$J$	$S/H_0$	$D/H_0$	$R_{ci}/H_0$	$R_t/H_0$	Area ratio	Configuration
5(a),(e)	9	26.4	0.5	0.25	0.5	$\infty$	1	ID jets
5(b),(c),(f),(g)	12	26.4	.5	.25	$\infty$	$\infty$	1	One-side
5(d),(h)	1	26.4	.5	.25	.5	$\infty$	1	OD jets
6(a),(e)	1	26.4	.5	.25	.5	$\infty$	1	OD jets
6(b),(c),(f)	18	26.4	1.0	.25	.5	$\infty$	1	Opposed, staggered
6(d),(g)	9	26.4	.5	.25	.5	$\infty$	1	ID jets
7(a),(c)	37	26.4	.25	.125	.5	$\infty$	1	Opposed, in-line
7(b),(d)	10	6.6	.5	.25	.5	$\infty$	1	Opposed, in-line
8(a),(d),(e)	30	6.6	.5	.25	$\infty$	$\infty$	1	Opposed, in-line
8(b),(f)	10	6.6	.5	.25	.5	$\infty$	1	Opposed, in-line
8(c),(g)	29	6.6	.5	.25	.25	$\infty$	1	Opposed, in-line
9(a),(c),(d)	21	6.6	.5	.25	$\infty$	1	1	Opposed, in-line
9(b),(e),(f)	30	6.6	.5	.25	$\infty$	$\infty$	1	Opposed, in-line
10(a),(d),(e)	31	6.6	.5	.25	$\infty$	$\infty$	1/3	Opposed, in-line
10(b),(f)	33	6.6	.5	.25	.25	$\infty$	1/3	Opposed, in-line
10(c),(g)	35	6.6	.5	.25	.25	2.2	1/3	Opposed, in-line
11(a),(c),(d)	41	26.4	.5	.25	$\infty$	0	1	One-side
11(b),(e),(f)	12	26.4	.5	.25	$\infty$	$\infty$	1	One-side

<sup>a</sup>From Refs. 29 and 30.

Not all combinations of the primary variables in the table were evaluated; only those combinations that are within the range given for the derived variables represent conditions that are within the validated range of the empirical model.

### Results and Discussion

The following discussion and analysis are parallel to the comparable sections in Ref. 28. To facilitate comparison with the previously published numerical results, the figures are similar in content, and the same color bars have been used to show the results from calculations with the empirical model. Unless noted to the contrary, observations made here for the empirical model results apply to the numerical model results also. It should be noted, however, that the empirical model calculations show more rapid mixing than the numerical model results. This is consistent with the numerical and empirical model comparisons shown in Ref. 12.

#### Differences Between ID and OD Injection Into a Curved Duct

Fig. 5 shows centerplane and cross-stream temperature contour plots downstream of a row of jets injected from the

inner (ID) and outer (OD) walls into a uniform mainstream flow in a nonconverging duct with a  $180^\circ$  turn. Orifice configuration A in Fig. 3 ( $S/H_0 = 0.5$ ;  $D/H_0 = 0.25$ ) was used for these calculations with the jet-to-mainstream momentum-flux ratio  $J$  equal to 26.4. This is an appropriate combination of orifice spacing and momentum-flux ratio for optimum mixing in a straight duct.<sup>10-12</sup> For comparison with the turning duct cases, contours calculated for a straight duct with the same jet flow and orifice geometry are also shown in this figure. The cross-stream plots for the straight duct case are shown at downstream distances equal to the distance along the injection wall at  $30^\circ$  into the turn for ID and OD injection, respectively.

Comparison of the centerplane view of injection from the ID wall in a curved duct with that in a straight channel (Figs. 5(a) and (b)) shows that the penetration is similar. Examination of the cross-stream plots in Figs. 5(e) and (f), however, shows that for ID injection into the curved duct the familiar kidney shape is not evident; that is, for ID injection the minimum temperature at any radius is on the centerplane ( $z/S = 0$ ), whereas for OD injection and straight-duct flows the minimum temperature is often off the centerplane.

Figs. 5(c) and (d) and 5(g) and (h) show a comparison of OD injection upstream of a 180° turn with injection into a straight duct. (Figs. 5(c) and (g) are from the same straight duct calculation shown in parts (b) and (f), with the plots inverted to facilitate comparison with the OD injection case.) For OD injection, the penetration and mixing are similar to that in a straight duct.

Figures 5(e) and (h) show that the jet structure and mixing are significantly different for the ID and OD jets. Note also that the jet trajectories drift slightly toward the ID wall of the turn compared to where they would be in a straight duct. This latter result was observed in the numerical calculations in Ref. 29 and in the experimental results in Refs. 26 and 27. It is not unexpected, since in the absence of any jets the mainstream flow would establish a free vortex in the turn, with radially increasing pressure and attendant inflow.

#### Opposed Rows with Jet Centerlines Staggered

It was reported in Refs. 10 and 12 that enhanced mixing was obtained when alternate jets for “optimum” one-side injection were moved to the opposite wall, creating opposed rows of jets with centerlines staggered. For example, if configuration A is selected to optimize the mixing for one side injection, then configurations B and C would be appropriate choices for opposite sides of the duct in an opposed-row, staggered jet configuration. The analogous situation in a turning duct is shown in Fig. 6. Jet centerline and cross-stream contour plots for the opposed-row configuration are shown in Figs. 6(b), (c), and (f). Note that parts (b) and (c) show planes through the OD and ID jets, respectively. Corresponding plots for separate rows of OD and ID jets are shown in parts (a) and (e), and (d) and (g), respectively.

These contours show that both the OD and ID jets in the opposed-row, staggered jets configuration penetrate farther than the comparable single-side case. This was also seen in the straight duct case.<sup>12</sup> A difference between the cross-stream shape of the OD and ID jets is apparent also, and is consistent with the corresponding contours of the separate OD and ID jet configurations.

#### Opposed Rows with Jet Centerlines In-line

An alternative to staggered centerlines in the opposed-row configuration is to have the centerlines directly opposed. To maintain the appropriate ratio of orifice spacing to mixing height for this case, the orifice spacing must be halved since the effective mixing height is half the height of the duct.<sup>10-12,31</sup> Since there will be four times as many injection locations for opposed, in-line injection, the orifice diameters must be half of that for the single-side case if the same flow split is desired. This is shown in configuration D ( $S/H_0 = 0.25$ ,  $D/H_0 = 0.125$ ) in Fig. 3. Centerplane and cross-stream contour plots for this configuration with  $J = 26.4$  are shown in Figs. 7(a) and (c).

A lower jet-to-mainstream momentum-flux ratio requires a greater orifice spacing to maintain optimum mixing. Centerplane and cross-stream temperature contours for configuration A with  $J = 6.6$  for opposed rows of in-line jets are shown in Figs. 7(b) and (d). The similarity of the flow pattern for coupled spacing and momentum-flux ratio is evident in comparing parts (b) and (d) for  $J = 6.6$  and  $S/H_0 = 0.5$  with parts (a) and (c) for  $J = 26.4$  and  $S/H_0 = 0.25$ . This similarity was also seen in the experimental and analytical results for opposed rows of in-line jets injected into a straight duct.<sup>12</sup>

#### Effects of Curvature in the $x-r$ Plane

The effect of varying the radius of curvature  $R_{ci}$  is shown in Fig. 8. Figs. 8(b) and (f) and 8(c) and (g) are centerplane and cross-stream contours for an ID radius of curvature equal to  $\frac{1}{2}$  and  $\frac{1}{4}$  times the height of the inlet duct (i.e.,  $R_{ci}/H_0 = 0.5$  and  $R_{ci}/H_0 = 0.25$ , respectively). The jet-to-mainstream momentum-flux ratio is 6.6 with an opposed-row, in-line jets configuration with  $S/H_0 = 0.5$  and  $D/H_0 = 0.25$  (configuration A). Both the centerplane and cross-stream distributions for these two radii of curvature are similar. For comparison, centerplane and cross-stream contour plots for the comparable straight duct case are shown in Figs. 8(a), (d), and (e). As in previous figures the straight and turning duct flows are similar, but the asymmetry of the mixing of the ID and OD jets is evident in both the turning duct cases.

#### Mixing of Jets in an Annular Duct (Effects of Curvature in the $r-z$ Plane)

The centerplane and cross-stream contours for a straight annulus and a comparable rectangular duct are shown in Fig. 9. Cross-section contours are shown at downstream distances of  $x/H_0 = 0.25$  and  $0.75$  for both the annular and rectangular ducts.

For the annular duct, the inside radius (ID) of the annulus was equal to the duct height (i.e.,  $R_i/H_0 = 1$ ). The orifice geometry was again an opposed-row, in-line jets configuration (A) with  $J = 6.6$ . Similar penetration and mixing, as seen in both the centerplane and cross-stream contours, was achieved by specifying the jet spacing for the annular duct to be equal to that in the rectangular duct at the radius which divides the annulus into equal areas.

#### Convergence Effects

The effect of a 1:3 (exit-to-inlet) area ratio convergence in straight and turning ducts is shown in the centerplane and cross-stream contours in Fig. 10 for the opposed-row, in-line jets configuration. In the case of the turning duct, this convergence may be obtained through reduction in the duct height or by circumferential convergence if the exit annulus is at a smaller radius (closer to the engine centerline) than the inlet. Centerplane and cross-stream temperature contours for these cases are shown in Figs. 10(b) and (f) and 10(c) and

(g), respectively. Temperature distributions, especially the cross-stream contours, are similar for both radial and circumferential convergence.

### Jets Injected Into a Can

This is the limiting case for OD injection with curvature in the  $r$ - $z$  plane where the radius of curvature of the inner annulus is equal to 0. Temperature contours for jet injection into a section of a can are shown in Figs. 11(a), (c), and (d). As in the case of the annular duct, cross-stream contours are shown at downstream distances of  $x/H_0 = 0.25$  and  $0.75$ . The corresponding centerplane and cross-stream contours for the rectangular duct case are shown in Figs. 11(b), (d), and (e), respectively.

The jet-to-mainstream momentum-flux ratio was 26.4. The jet spacing for this case was specified, at the radius which divides the can into equal areas, as that appropriate for injection of a row of jets into a rectangular duct. That is, the relationship of the spacing between jet centerlines to the number of holes around the circumference of the can would be

$$S = 2\pi R_{1/2}/n \quad (3)$$

where

$$R_{1/2} = H_0/\sqrt{2} \quad (4)$$

Substituting these into the spacing and momentum-flux relationship for a rectangular duct<sup>12</sup>

$$C = (S/H_0) \sqrt{J} \quad (5)$$

gives the appropriate number of holes as

$$n = \pi\sqrt{2J}/C \quad (6)$$

It follows that each sector would be  $360/n$  degrees.

### Limitations and Applicability

Examination of the empirical model results in Ref. 12 shows that correlation of experimental data can provide a good predictive capability within the parameter range of the generating experiments, provided that the experimental results are consistent with the assumptions made in the empirical model. These models must, however, be used with caution, or not at all, outside this range.

Use of the empirical model in regions close to the injection location ( $x/D < 1$ ) is not recommended. It should also be noted that the form of the empirical correlations in the current model (and previous versions in Refs. 5 and 11) precludes their use for semi-confined flows (large  $H_0/D$  or  $S/D$ ), single jet flows,

or flows in which it is known a priori that the primary assumptions in the model will be invalid.

### Summary of Results

An existing empirical model for the temperature field downstream of single and multiple rows of jets injected into a confined crossflow has been extended to model the effects of curvature and convergence on the mixing. This extension is based on the results of a numerical study of these effects using a three-dimensional turbulent flow computer code. Temperature distributions calculated with the empirical model are presented to show the effects of flow area convergence, radius of curvature, and inner and outer wall injection for single and opposed rows of jets.

The following conclusions can be made from the results:

1. Transition duct curvature causes a drift of the jet trajectories toward the inner wall. The different structures for the ID and OD jets, observed in the calculations with the numerical model, are shown in calculations with the empirical model also.

2. Jet penetration and mixing in a turning and converging duct are similar to the effects seen in a converging straight channel, namely that the optimum orifice spacing and momentum-flux relationships are unchanged, and the mixing is not inhibited by the convergence. This appears to be independent of whether the convergence in the turning duct is radial or circumferential.

3. Jet trajectories in an annulus (or can) are similar to those in a rectangular duct for the same jet-to-mainstream momentum-flux and orifice-spacing-to-duct-height (radius) ratios provided that the spacing is specified at the radius dividing the annulus (or can) into equal areas.

### Appendix—Correlation Equations

#### Jet Thermal Centerline Trajectory

$$y_c/H_{eq} = 0.3575 a_1 J^{0.25} (S/D)^{0.14} (H_{eq}/D)^{-0.45} \\ \times C_d^{0.155} (x/H_{eq})^{0.17} \exp(-b)$$

where

$$a_1 = \min[(1 + S/H_{eq}), 2]$$

and

$$b = 0.091 (x/H_{eq})^2 [(H_{eq}/S)^2 - (\sqrt{J}/3.5)]$$

### Centerplane Maximum Temperature Difference Ratio

$$\theta_c = \theta_{EB} + (1 - \theta_{EB}) \left[ a_1 J^{-0.35} C_d^{0.5} (H_{eq}/D)^{-1} (x/H_{eq})^{-1} \right]^f$$

where

$$f = 1.15 \sqrt{(S/H_{eq})/(1 + S/H_{eq})}$$

and

$$\theta_{EB} = w_j/w_T$$

### Centerplane Minimum Temperature Difference Ratios

$$\theta_{\min}^+/\theta_c = 1 - \exp(-c^+)$$

where

$$c^+ = 0.038 a_3 J^{1.62} (S/D)^{1.5} (H_{eq}/D)^{-2.57} C_d^{0.535} (x/H_{eq})^{1.1}$$

and

$$a_3 = 1 \quad \text{if} \quad \left[ (y_c/H_{eq}) + (W_{1/2}^+/H_{eq}) \right] \leq 1$$

$$= (H_0/H_{eq})^{3.67} \quad \text{if} \quad \left[ (y_c/H_{eq}) + (W_{1/2}^+/H_{eq}) \right] > 1$$

$$\theta_{\min}^-/\theta_c = 1 - \exp(-c^-)$$

where

$$c^- = Q a_4 J^{-0.3} (S/D)^{-1.4} (H_{eq}/D)^{0.9} C_d^{0.25} (x/H_{eq})^{0.9}$$

and

$$a_4 = 1.57 \quad \text{if} \quad R_{ci}/H_{eq} = \infty \quad (\text{straight duct})$$

$$= 3.93 \quad \text{if} \quad R_{ci}/H_{eq} < \infty \quad (\text{curved duct})$$

$$Q = 1 \quad \text{if} \quad \left[ (y_c/H_{eq}) + (W_{1/2}^+/H_{eq}) \right] \leq 1 \quad \text{or} \quad R_{ci}/H_{eq} < \infty$$

$$= \exp \left\{ 0.22 (x/H_{eq})^2 \left[ (\sqrt{J/5}) - (S/H_{eq}) \right] \right\}$$

$$\text{if} \quad \left[ (y_c/H_{eq}) + (W_{1/2}^+/H_{eq}) \right] > 1 \quad \text{and} \quad R_{ci}/H_{eq} = \infty$$

### Centerplane Half-Widths

$$W_{1/2}^+/H_{eq} = a_5 J^{0.18} (S/D)^{-0.25} (H_0/H_{eq})^{0.5} C_d^{0.125} (x/H_{eq})^{0.5}$$

where

$$a_5 = 0.1623 \quad \text{if} \quad R_{ci}/H_{eq} = \infty \quad (\text{straight duct})$$

$$= 0.3 \quad \text{if} \quad R_{ci}/H_{eq} < \infty \quad (\text{curved duct})$$

$$W_{1/2}^-/H_{eq} = a_6 J^{0.15} (S/D)^{0.27} (H_{eq}/D)^{-0.38} (H_0/H_{eq})^{0.5}$$

$$\times C_d^{0.055} (x/H_{eq})^{0.12}$$

where

$$a_6 = 0.20 \quad \text{if} \quad R_{ci}/H_{eq} = \infty \quad (\text{straight duct})$$

$$= 0.5 \quad \text{if} \quad R_{ci}/H_{eq} < \infty \quad (\text{curved duct})$$

### Off-Centerplane Thermal Trajectory

$$y_{c,z}/y_c = 1 - \left[ 4(z/S)^2 \exp(-g) \right]$$

where

$$g = 0.227 J^{0.67} (S/D)^{-1} (H_{eq}/D)^{0.54} C_d^{0.23} (x/H_{eq})^{0.54}$$

### Off-Centerplane Maximum Temperature Difference Ratio

$$\theta_{c,z}/\theta_c = 1 - \left[ 4(z/S)^2 \exp(-d) \right]$$

where

$$d = 0.452 J^{0.53} (S/D)^{-1.53} (H_{eq}/D)^{0.83} C_d^{0.35} (x/H_{eq})^{0.83}$$

### Off-Centerplane Minimum Temperature Difference Ratio

$$\theta_{\min,z}^\pm/\theta_{c,z} = \theta_{\min}^\pm/\theta_c$$

### Off-Centerplane Half-Widths

$$W_{1/2,z}^\pm/H_{eq} = W_{1/2}^\pm/H_{eq}$$

The six scaling parameters,  $y_c/H_{eq}$ ,  $\theta_c$ ,  $\theta_{\min}^+$ ,  $\theta_{\min}^-$ ,  $W_{1/2}^+/H_{eq}$ , and  $W_{1/2}^-/H_{eq}$ , are used in Eq. (3) to define the vertical profile at any  $x, z$  location in the flow. For all except the case of opposed rows of jets with centerlines in-line,  $H_{eq}$  in the correlation equations is equal to  $H_0$ , the height of the duct at the injection location.

### Nonisothermal Mainstream

#### Double (Axially Staged) Rows of Jets

#### Opposed Rows of Jets with Centerlines Staggered

It was shown in Ref. 12 that these flows can be satisfactorily modeled by superimposing independent calculations of the separate elements. This is accomplished as follows:

$$\theta = [\theta_1 + \theta_2 - (2\theta_1\theta_2)]/[1 - (\theta_1\theta_2)]$$

Note that  $\theta = \theta_1$  at any location where  $\theta_2 = 0$  (and  $\theta = \theta_2$  if  $\theta_1 = 0$ ); and that  $\theta \leq 1$  (provided that  $\theta_1$  and  $\theta_2$  are each  $\leq 1$ ). Also, for the completely mixed case  $\theta_{EB}$  is equal to the ratio of the total jet flow to the mainstream flow as required.

### Opposed Rows of Jets With Centerlines In-Line

It was observed in Ref. 2 that the flowfield downstream of opposed jets was similar to that downstream of a single jet injected toward an opposite wall at half the distance between the jets. This is also confirmed by the experimental results in Ref. 17. Thus for the symmetric case,  $H_{eq} = H_0/2$ .

In general, these flows can be modeled by calculating an effective duct height as proposed in Ref. 9, namely

$$(H_{eq})_{top} = H_0 \frac{[(A_j/A_m)\sqrt{J}]_{top}}{[(A_j/A_m)\sqrt{J}]_{top} + [(A_j/A_m)\sqrt{J}]_{bottom}}$$

and

$$(H_{eq})_{bottom} = H_0 - (H_{eq})_{top}$$

### Effects Due to Curvature

The flow in a curved duct develops a free vortex, wherein  $U = (\text{const})/r$ , with higher velocities near the inner wall than near the outer wall. The local momentum flux ratio is thus

$$J_{local} = 4J[r/(r_i + r_o)]^2$$

where  $J$  is the momentum flux ratio based on the uniform mainstream velocity.

The effective momentum flux ratio for OD jets is defined to be the integrated average of the values of  $J_{local}$  over the outer half of the duct, and similarly the effective momentum flux ratio for ID jets is defined to be the integrated average of the  $J_{local}$  values over the inner half of the duct. These values are

$$J_{OD} = J(1 + 2C_{OD} + 4C_{OD}^2)/3$$

$$J_{ID} = J(1 + 2C_{ID} + 4C_{ID}^2)/3$$

where

$$C_{OD} = (1 + H_0/R_{ci})/(2 + H_0/R_{ci})$$

and

$$C_{ID} = 1/(2 + H_0/R_{ci})$$

### Flow Area Convergence

This case is modeled by assuming that the accelerating mainstream will act to decrease the effective momentum flux ratio as the flow proceeds downstream, thus

$$J(x) = J[H(x)/H_0]^2$$

Note that the trajectory and the jet half-widths are calculated in terms of the duct height at the injection location, so must be scaled by the inverse of the convergence rate  $H_0/H(x)$  to give profiles in terms of the local duct height.

### Orifice Aspect Ratio

It was observed in Ref. 18 that bluff slots resulted in slightly less jet penetration and more two-dimensional profiles than circular holes, and that streamlined slots resulted in slightly greater jet penetration and more three-dimensional profiles. This effect is modeled by using the ratio of the orifice spacing to the orifice width  $S/W$  in lieu of  $S/D$  in the correlation equations. For rectangular orifices with circular ends

$$S/W = (S/D)\sqrt{1 + (4/\pi)(AR - 1)} \quad \text{if } AR > 1$$

and

$$S/W = (S/D)\sqrt{1 + (4/\pi)(1/AR - 1)} / AR \quad \text{if } AR < 1$$

$$AR = W/L$$

### Slanted Slots

Two effects were noted in the experimental results for slanted slots, namely that the centerplanes shifted laterally with increasing downstream distance, and the axes of the kidney-shaped temperature contours were inclined with respect to the injection direction. The former is modeled as a function of momentum flux ratio and downstream distance as

$$dz/S = \sin[(\pi/2)a]$$

where

$$a = \min\left[1, (x/H_{eq})(J/26.4)^{0.25}\right]$$

The rotation effect observed in the experimental data is not modeled.

### References

1. Holdeman, J.D., Walker, R.E., and Kors, D.L., "Mixing of Multiple Dilution Jets With a Hot Primary Airstream for Gas Turbine Combustors," AIAA Paper 73-1249, Nov. 1973. (NASA TM X-71426.)
2. Kamotani, Y., and Greber, I., "Experiments on Confined Turbulent Jets in Cross Flow," NASA CR-2392, 1974.
3. Cox, G.B., Jr., "An Analytical Model for Predicting Exit Temperature Profile from Gas Turbine Engine Annular Combustors," AIAA Paper 75-1307, Sept. 1975.
4. Cox, G.B., Jr., "Multiple Jet Correlations for Gas Turbine Engine Combustor Design," Journal of Engineering for Power, Vol. 98, No. 2, Apr. 1976, pp. 265-273.

5. Holdeman, J.D., and Walker, R.E., "Mixing of a Row of Jets with a Confined Crossflow," AIAA Journal, Vol. 15, No. 2, Feb. 1977, pp. 243-249.
6. Khan, Z.A., McGuirk, J.J., and Whitelaw, J.H., "A Row of Jets in a Crossflow," Fluid Dynamics of Jets With Applications to V/STOL, AGARD-CP-308, AGARD, Neuilly-Sur-Seine, France, 1982, pp. 10-1 to 10-11.
7. Holdeman, J.D., "Perspectives on the Mixing of a Row of Jets With a Confined Crossflow," AIAA Paper 83-1200, June 1983. (NASA TM-83457).
8. Atkinson, K.N., Khan, Z.A., and Whitelaw, J.H., "Experimental Investigation of Opposed Jets Discharging Normally into a Cross-Stream," Journal of Fluid Mechanics, Vol. 115, Feb. 1982, pp. 493-504.
9. Wittig, S.L.K., Elbahar, O.M.F., and Noll, B.E., "Temperature Profile Development in Turbulent Mixing of Coolant Jets with a Confined Hot Crossflow," Journal of Engineering for Gas Turbines and Power, Vol. 106, No. 1, Jan. 1984, pp. 193-197.
10. Holdeman, J.D., Srinivasan, R., and Berenfeld, A., "Experiments in Dilution Jet Mixing," AIAA Journal, Vol. 22, No. 10, Oct. 1984, pp. 1436-1443.
11. Holdeman, J.D., Srinivasan, R., Coleman, E.B., Meyers, G.D., and White, C.D., "Effects of Multiple Rows and Noncircular Orifices on Dilution Jet Mixing," Journal of Propulsion and Power, Vol. 3, No. 3, May-June 1987, pp. 219-226.
12. Holdeman, J.D., and Srinivasan, R., "Modeling Dilution Jet Flowfields," Journal of Propulsion and Power, Vol. 2, No. 1, Jan.-Feb. 1986, pp. 4-10.
13. Holdeman, J.D., and Srinivasan, R., "Perspectives on Dilution Jet Mixing," AIAA Paper 86-1611, June 1986. (NASA TM-87294.)
14. Walker, R.E., and Kors, D.L., "Multiple Jet Study," NASA CR-121217, 1973.
15. Walker, R.E., and Eberhardt, R.G., "Multiple Jet Study Data Correlations," NASA CR-134795, 1974.
16. Srinivasan, R., Berenfeld, A., and Mongia, H.C., "Dilution Jet Mixing Program, Phase I," GARRETT-21-4302, Garrett Turbine Engine Company, Phoenix, AZ, Nov. 1982. (NASA CR-168031.)
17. Srinivasan, R., Coleman, E., and Johnson, K., "Dilution Jet Mixing Program, Phase II," GARRETT-21-4804, Garrett Turbine Engine Company, Phoenix, AZ, June 1984. (NASA CR-174624.)
18. Srinivasan, R., Meyers, G., Coleman, E., and White, C., "Dilution Jet Mixing Program, Phase III," GARRETT-21-5418, Garrett Turbine Engine Company, Phoenix, AZ, Sept. 1985. (NASA CR-174884.)
19. Srinivasan, R., and White, C., "Dilution Jet Mixing Program, Supplementary Report," GARRETT-21-4705, Garrett Turbine Engine Company, Phoenix, AZ, Mar. 1986. (NASA CR-175043.)
20. Bruce, T.W., Mongia, H.C., and Reynolds, R.S., "Combustor Design Criteria Validation," Vols. 1-3, AIRESEARCH-75-211682(38)-1,-2,-3, AiResearch Manufacturing Co., Phoenix, AZ, Mar. 1979. (USARTL-TR-78-55A, -55B-VOL-2, and -55C-VOL-3: Avail. NTIS, AD-A067657, AD-A067689, and AD-A066793.)
21. Claus, R.W., "Analytical Calculation of a Single Jet in Crossflow and Comparison With Experiment," AIAA Paper 83-0238, Jan. 1983. (NASA TM-83027.)
22. Kenworthy, M.J., Correa, S.M., and Burrus, D.L., "Aerothermal Modeling, Phase I, Vol. 1—Model Assessment," NASA CR-168296-VOL-1, 1983.
23. Srinivasan, R., Reynolds, R., Ball, I., Berry, R., Johnson, K., and Mongia, H., "Aerothermal Modeling Program, Phase I—Vol. 2," GARRETT-21-4742-2, Garrett Turbine Engine Co., Phoenix, AZ, Aug. 1983. (NASA CR-168243-VOL-2.)
24. Sturgess, G.J., "Aerothermal Modeling Program, Phase I," PWA-5907-19, Pratt & Whitney Aircraft, East Hartford, CT, July 1983. (NASA CR-168202.)
25. Mongia, H.C., Reynolds, R.S., and Srinivasan, R., "Multidimensional Gas Turbine Combustion Modeling: Applications and Limitations," AIAA Journal, Vol. 14, No. 6, June 1986, pp. 890-904.
26. Lipshitz, A., and Greber, I., "Dilution Jets in Accelerated Cross Flows," NASA CR-174717, 1984.
27. Zizelman, J., "Dilution Jet Configurations in a Reverse Flow Combustor," M.S. Thesis, Case Western Reserve University, Cleveland, OH, 1985 (NASA CR-174888).
28. Holdeman, J.D., Reynolds, R., and White, C., "A Numerical Study of the Effects of Curvature and Convergence on Dilution Jet Mixing," AIAA Paper 87-1953, June 1987. (NASA TM-89878.)
29. Reynolds, R., and White, C., "Transition Mixing Study," GARRETT-21-5723, Garrett Turbine Engine Company, Phoenix, AZ, 1987. (NASA CR-175062.)
30. Srinivasan, R., and White, C., "Transition Mixing Study Empirical Model Report," GARRETT-21-6689, Garrett Engine Division, Phoenix, AZ, 1988, (NASA CR-182139.)
31. Holdeman, J.D., "Experiments and Modeling of Dilution Jet Flowfields," NASA-Chinese Aeronautical Establishment (CAE) Symposium, NASA CP-2433, 1986, pp. 149-174.

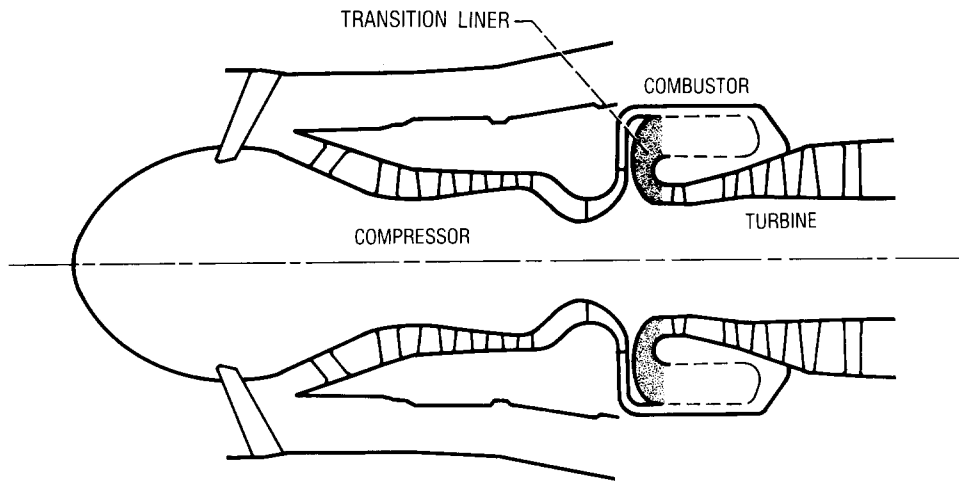


Fig. 1 Schematic of gas turbine engine with reverse-flow combustor configuration.

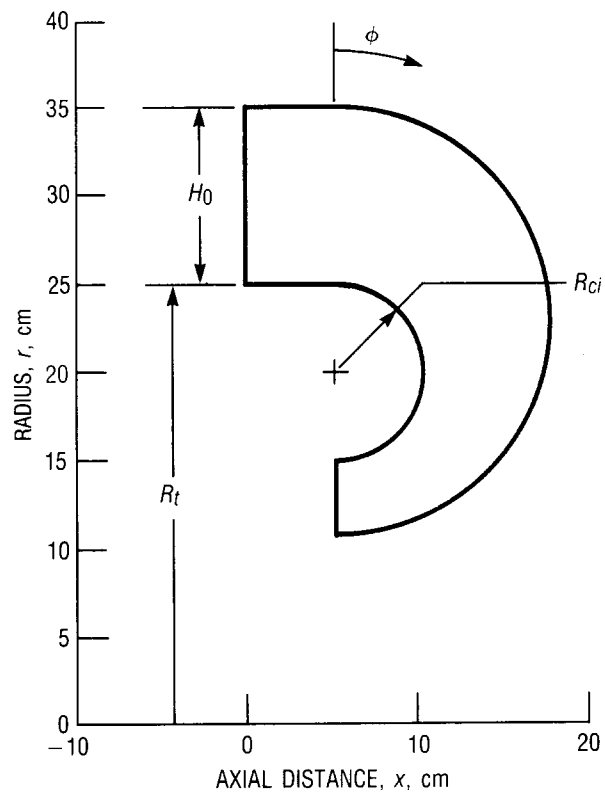


Fig. 2 Transition duct geometry.

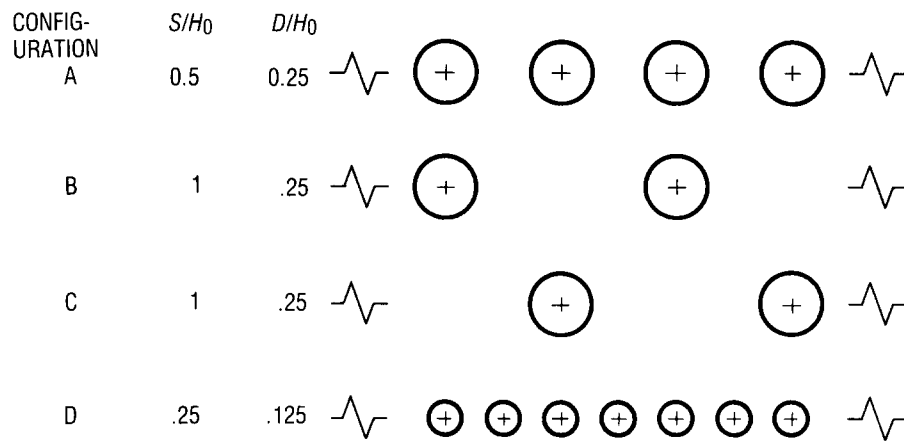


Fig. 3 Orifice configurations.

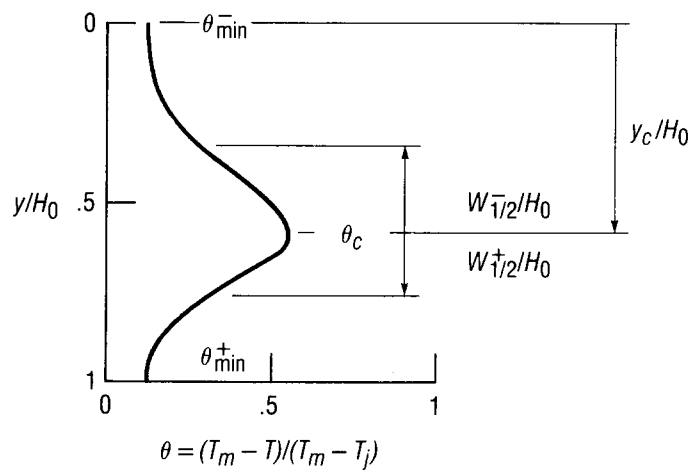


Fig. 4 Typical vertical temperature profile showing scaling parameters in empirical model.

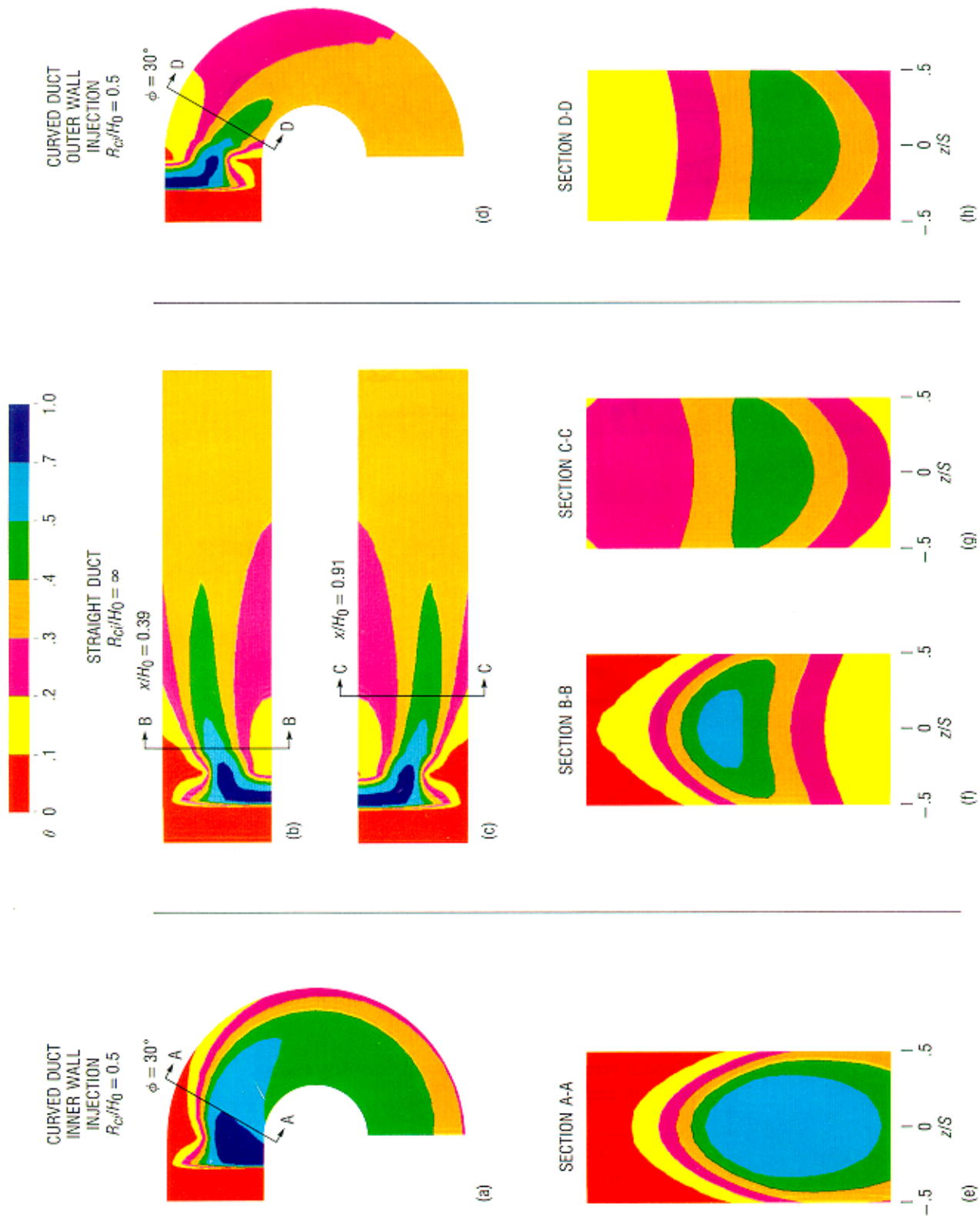


Fig. 5 Comparison of duct shapes and injection sites. All axial views at  $z/S = 0$ ,  $J = 26.4$ ,  $S/H_0 = 0.5$ ,  $D/H_0 = 0.25$ ,  $R_i/H_0 = \infty$ .

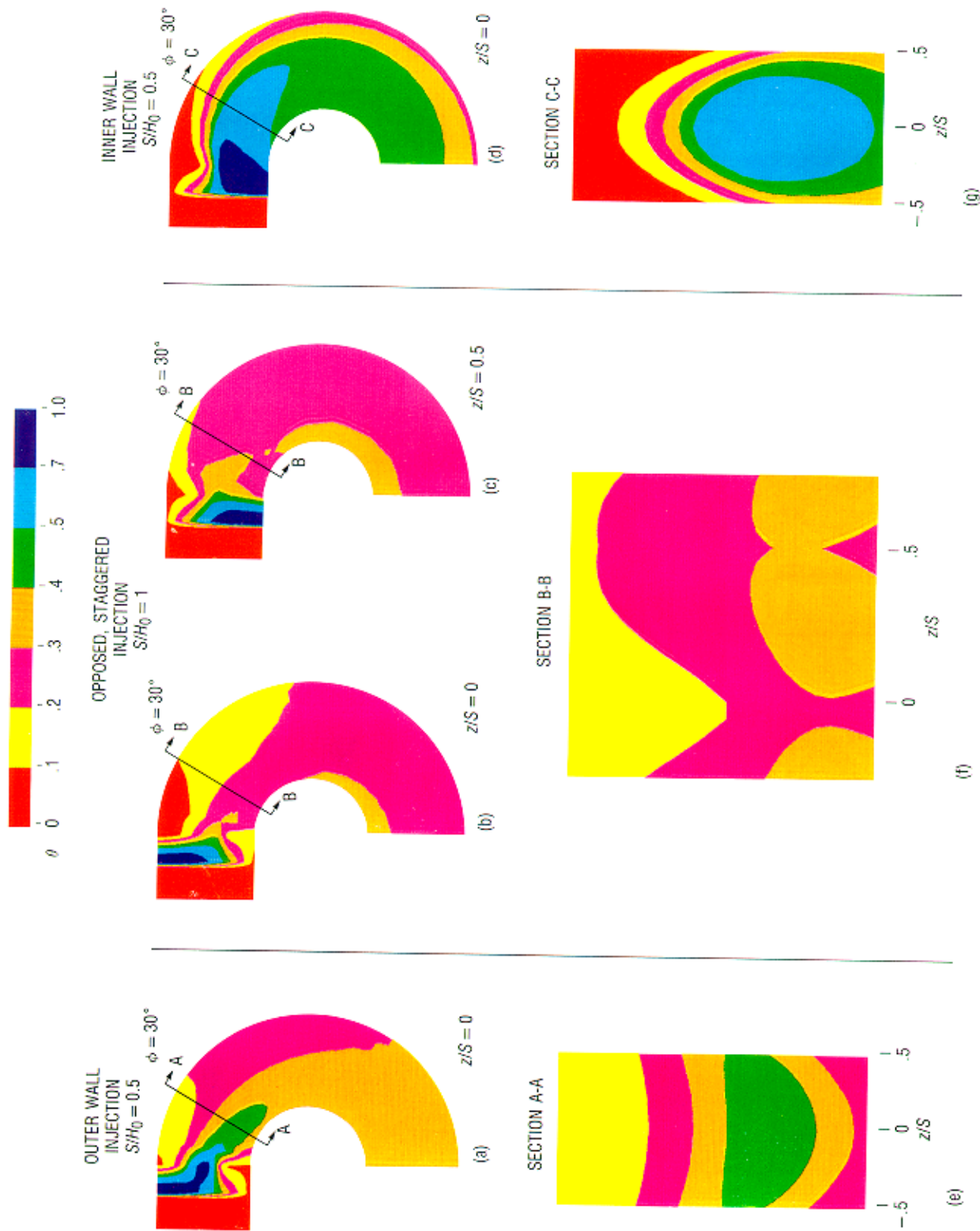


Fig. 6 Opposed rows with jet centerlines staggered.  $J = 26.4$ ,  $D/H_0 = 0.25$ ,  $R_c/H_0 = 0.5$ ,  $R_f/H_0 = \infty$ .

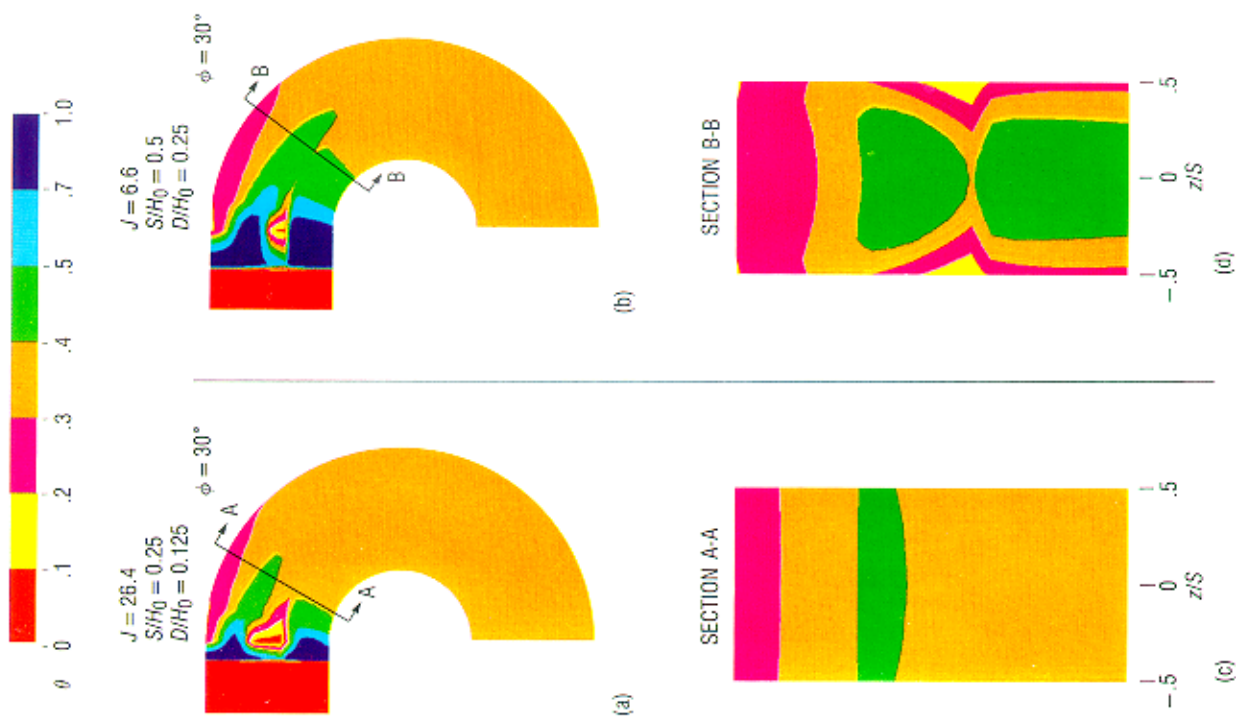


Fig. 7 Opposed rows with jet centerlines in-line. All axial views at  $z/S = 0$ ,  $R_{ci}/H_0 = 0.5$ ,  $R_i/H_0 = \infty$ .

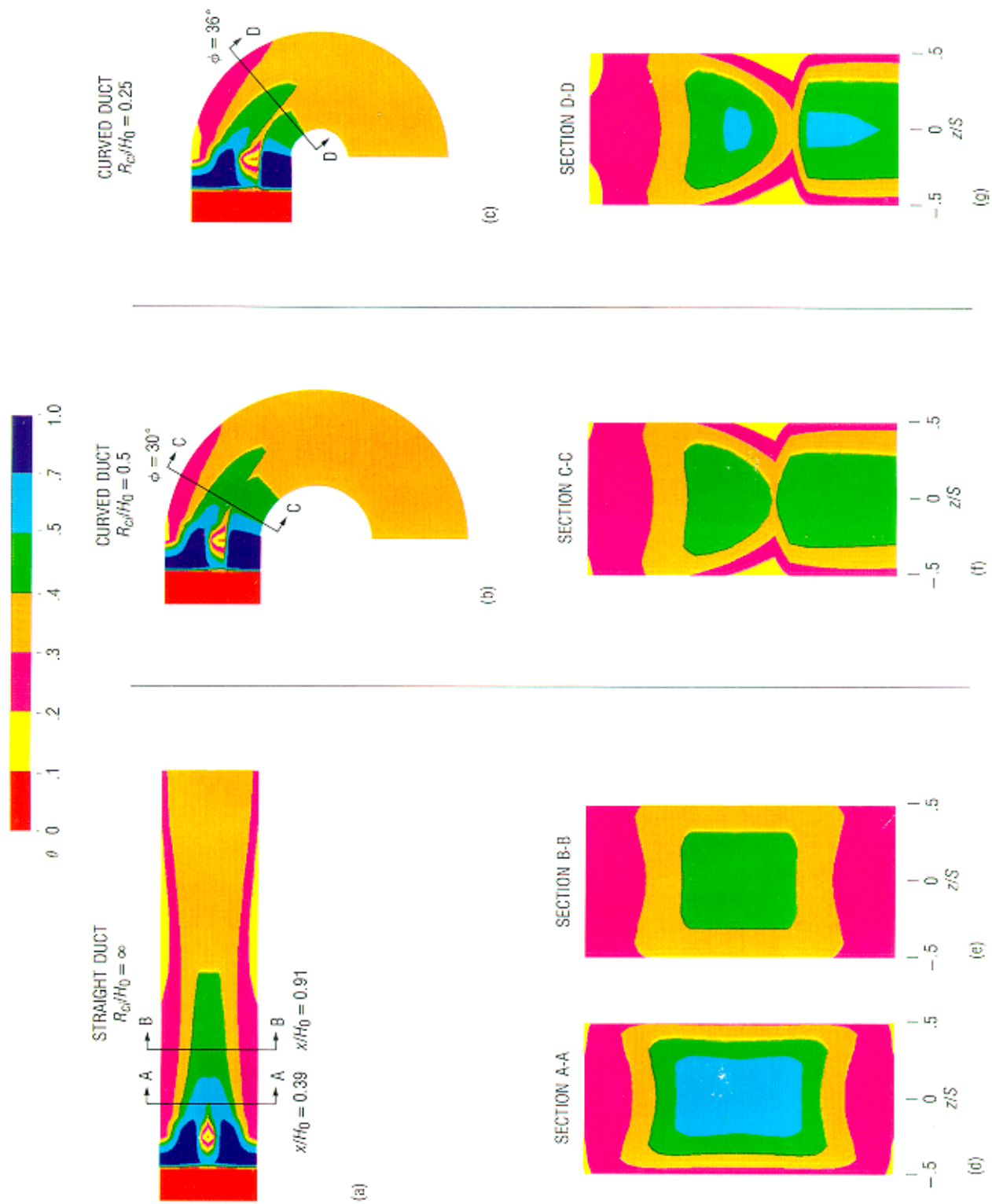


Fig. 8 Effect of radius of curvature in  $x-r$  plane. All axial views at  $z/S = 0$ ,  $J = 6.6$ ,  $S/H_0 = 0.5$ ,  $D/H_0 = 0.25$ ,  $R_c/H_0 = \infty$ .

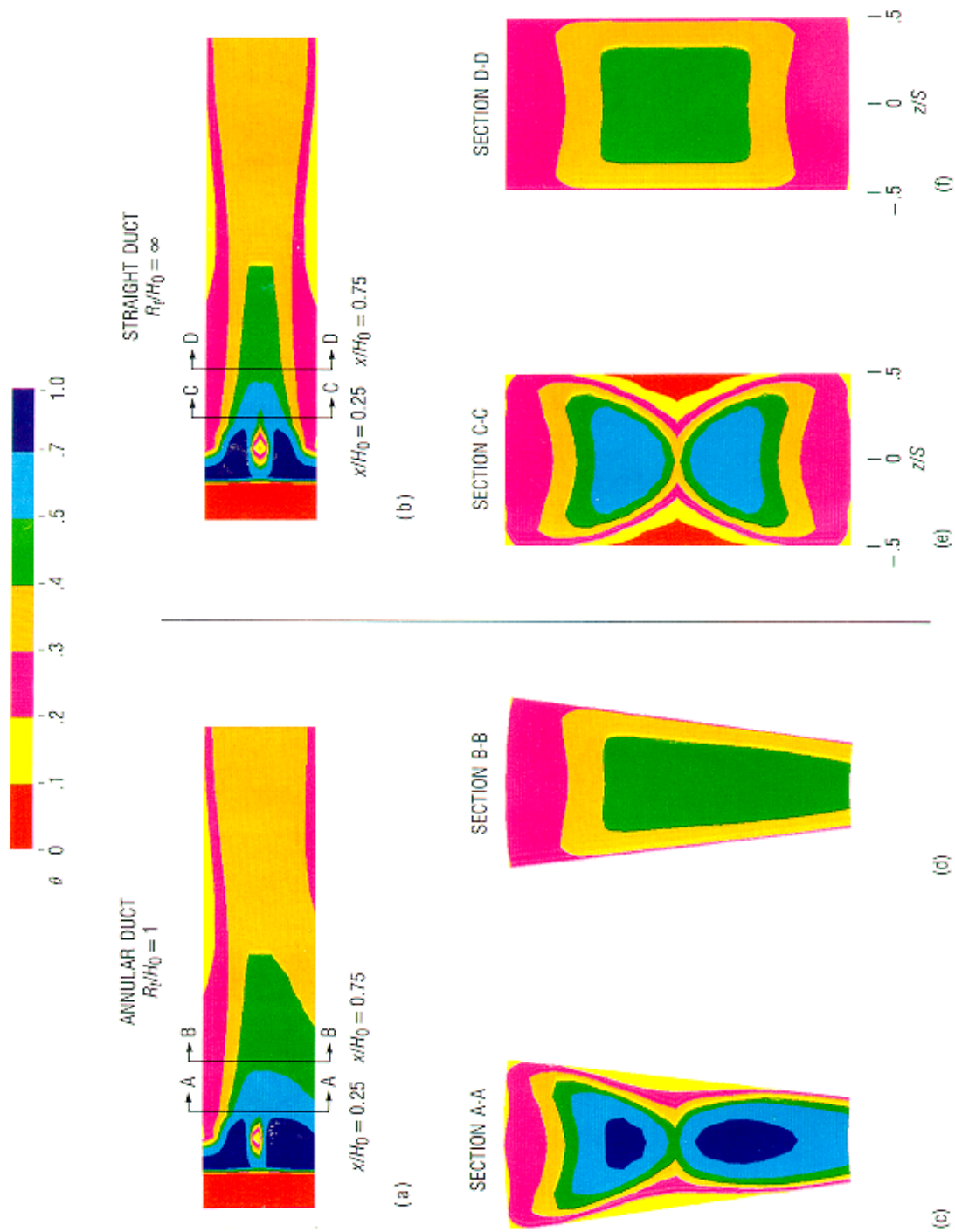


Fig. 9 Mixing of jets in annular duct. All axial views at  $z/S = 0$ ,  $J = 6.6$ ,  $S/H_0 = 0.5$ ,  $D/H_0 = 0.25$ ,  $R_{ci}/H_0 = \infty$ .

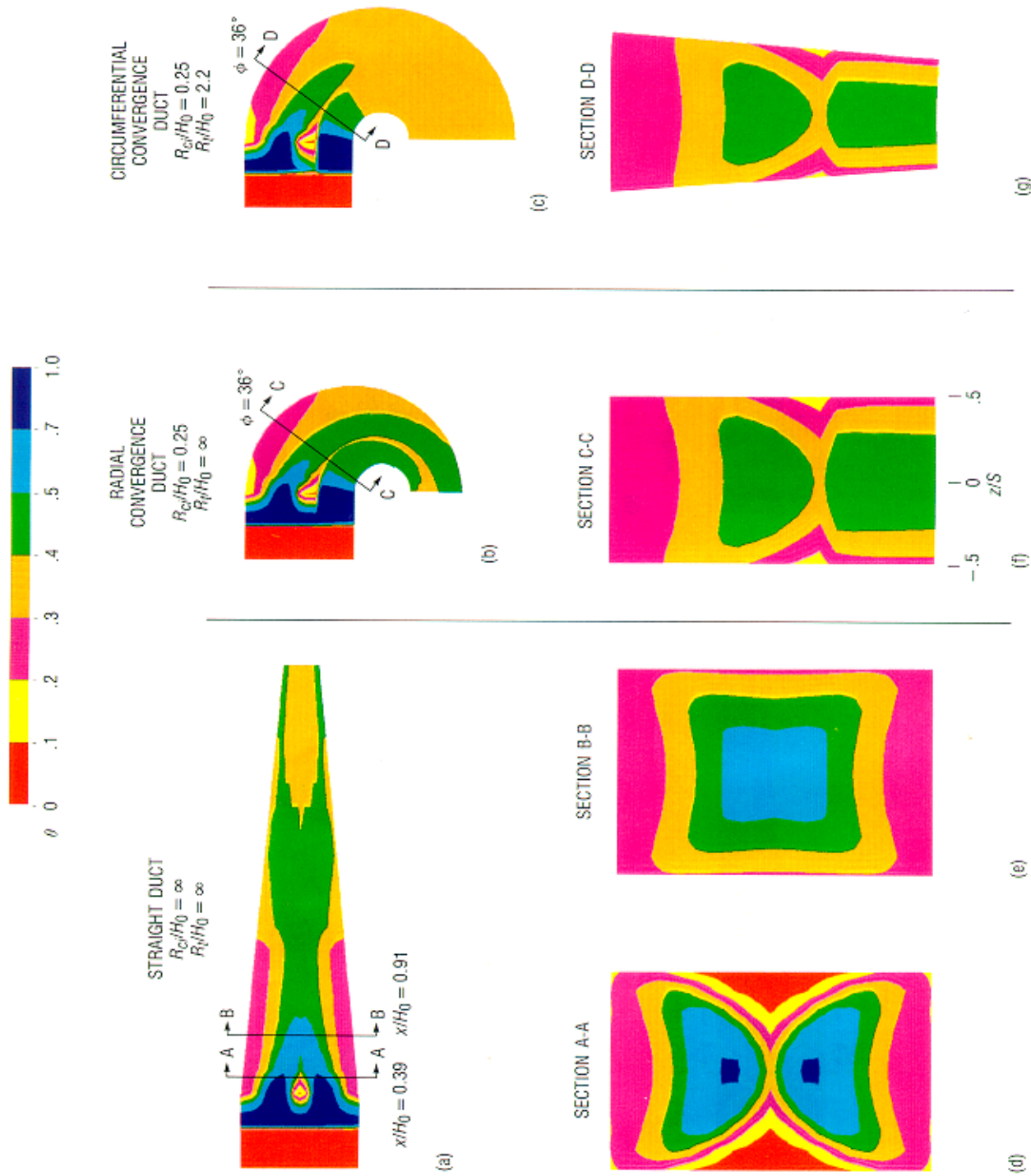


Fig. 10 Effect of convergence. All axial views at  $z/S = 0$ ,  $J = 6.6$ ,  $S/H_0 = 0.5$ ,  $D/H_0 = 0.25$ .

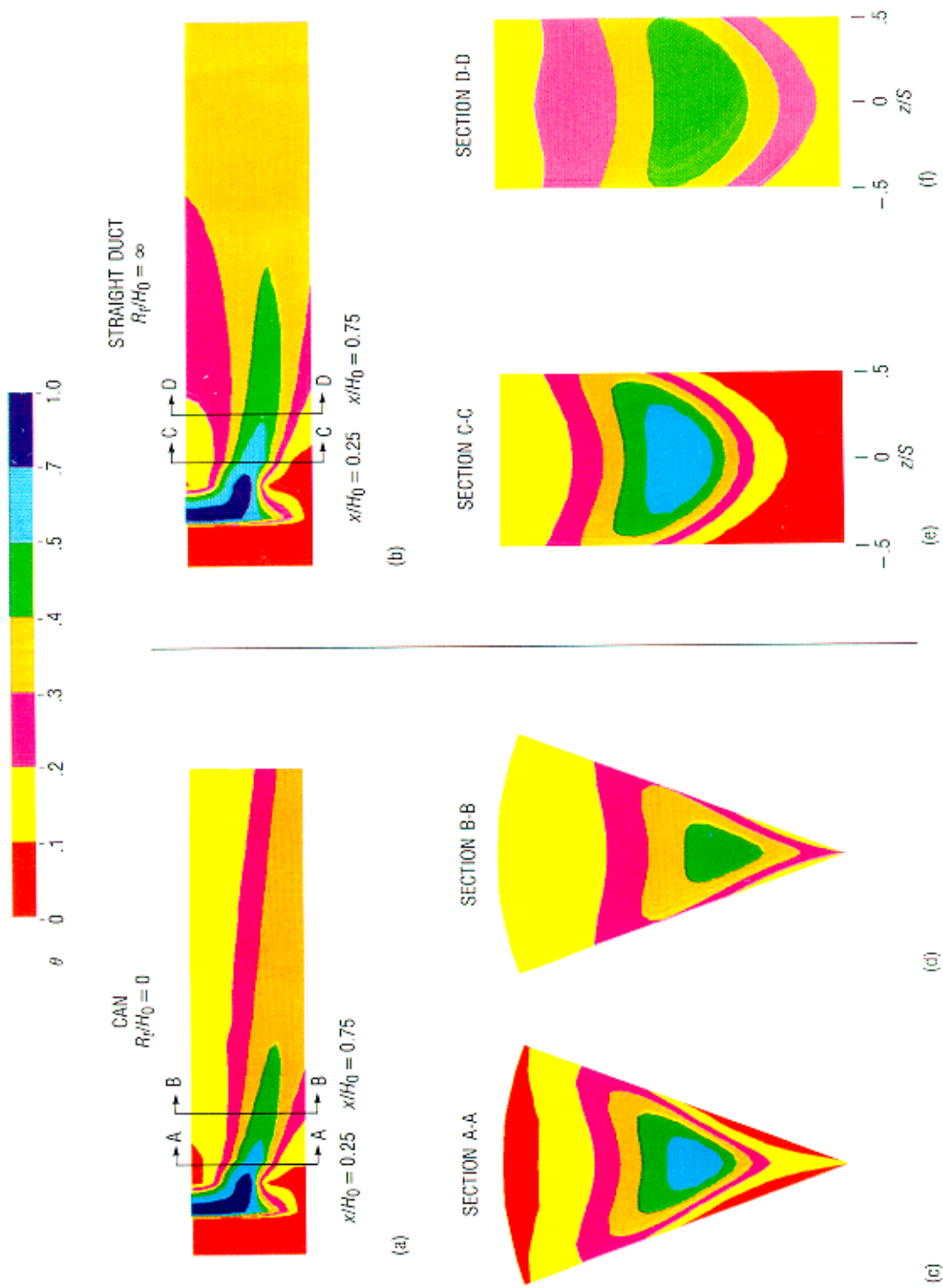


Fig. 11 Jets injected into can. All axial views at  $z/S = 0$ ,  $J = 26.4$ ,  $S/H_0 = 0.5$ ,  $D/H_0 = 0.25$ ,  $R_0/H_0 = \infty$ .

**REPORT DOCUMENTATION PAGE**Form Approved  
OMB No. 0704-0188

Public reporting burden for this collection of information is estimated to average 1 hour per response, including the time for reviewing instructions, searching existing data sources, gathering and maintaining the data needed, and completing and reviewing the collection of information. Send comments regarding this burden estimate or any other aspect of this collection of information, including suggestions for reducing this burden, to Washington Headquarters Services, Directorate for Information Operations and Reports, 1215 Jefferson Davis Highway, Suite 1204, Arlington, VA 22202-4302, and to the Office of Management and Budget, Paperwork Reduction Project (0704-0188), Washington, DC 20503.

<b>1. AGENCY USE ONLY (Leave blank)</b>		<b>2. REPORT DATE</b> July 1988	<b>3. REPORT TYPE AND DATES COVERED</b> Technical Memorandum	
<b>4. TITLE AND SUBTITLE</b> An Empirical Model of the Effects of Curvature and Convergence on Dilution Jet Mixing			<b>5. FUNDING NUMBERS</b>  WU-505-62-21-00	
<b>6. AUTHOR(S)</b> James D. Holeman, Ram Srinivasan, and Craig D. White				
<b>7. PERFORMING ORGANIZATION NAME(S) AND ADDRESS(ES)</b> National Aeronautics and Space Administration Lewis Research Center Cleveland, Ohio 44135-3191			<b>8. PERFORMING ORGANIZATION REPORT NUMBER</b>  E-4143	
<b>9. SPONSORING/MONITORING AGENCY NAME(S) AND ADDRESS(ES)</b> National Aeronautics and Space Administration Washington, DC 20546-0001			<b>10. SPONSORING/MONITORING AGENCY REPORT NUMBER</b>  NASA TM-100896 AIAA-88-3180	
<b>11. SUPPLEMENTARY NOTES</b>  Prepared for the 24th Joint Propulsion Conference cosponsored by the AIAA, ASME, SAE, and ASEE, Boston, Massachusetts, July 11-13, 1988. James D. Holdeman, NASA Lewis Research Center; Ram Srinivasan and Craig D. White, Allied-Signal Aerospace Company, Garrett Engine Division, Phoenix, Arizona.				
<b>12a. DISTRIBUTION/AVAILABILITY STATEMENT</b> Unclassified - Unlimited Subject Categories: 07  Available electronically at <a href="http://gltrs.grc.nasa.gov/GLTRS">http://gltrs.grc.nasa.gov/GLTRS</a> This publication is available from the NASA Center for AeroSpace Information, 301-621-0390.			<b>12b. DISTRIBUTION CODE</b>	
<b>13. ABSTRACT (Maximum 200 words)</b>  An existing empirical model for the temperature field downstream of single and multiple rows of jets injected into a confined crossflow has been extended to model the effects of curvature and convergence on the mixing. This extension is based on the results of a numerical study of these effects using a three-dimensional turbulent flow computer code. Temperature distributions calculated with the empirical model are presented to show the effects of flow area convergence, radius of curvature, and inner and outer wall injection for single and opposed rows of jets.				
<b>14. SUBJECT TERMS</b> Dilution jet mixing; Transition liner; Gas turbine combustor			<b>15. NUMBER OF PAGES</b> 20	
			<b>16. PRICE CODE</b> A02	
<b>17. SECURITY CLASSIFICATION OF REPORT</b> Unclassified	<b>18. SECURITY CLASSIFICATION OF THIS PAGE</b> Unclassified	<b>19. SECURITY CLASSIFICATION OF ABSTRACT</b> Unclassified	<b>20. LIMITATION OF ABSTRACT</b>	